Effect of Microstructure on the Static and Dynamic Behavior of Recycled Asphalt Material

Martin H. Sadd, Arun Shukla,
Venkitanarayanan Parameswaran and Qingli Dai
University of Rhode Island

February 2004

URITC PROJECT NO. 536164

PREPARED FOR

UNIVERSITY OF RHODE ISLAND
TRANSPORTATION CENTER

1. Report No	2. Government Accession No.	3. Recipient's Catalog No.
URITC FY 01-14	N/A	N/A

4. Title and Subtitle	5. Report Date
Effect of Microstructure on the Static and Dynamic Behavior of Recycled Asphalt Materials	February 2004
	6. Performing Organization Code N/A
7. Authors(s) Martin H. Sadd, Arun Shukla, Venkit Parameswaran and Qingli Dai	8. Performing Organization Report No.
9. Performing Organization Name and Address University of Rhode Island Mechanical Engineering & Applied Mechanics Department 92 Upper College Road Kingston, RI 02881	10. Work Unit No. (TRAIS) N/A 11. Contract or Grant No. 536164 13. Type of Report and Period Covered Final
12. Sponsoring Agency Name and Address University of Rhode Island Transportation Research Center Kingston, RI 02881	14. Sponsoring Agency Code

15. Supplementary Notes
N/A

16. Abstract

This report describes the third year's research activities of a project dealing with the micromechanical behavior of asphalt materials. The project involved both theoretical/numerical modeling and experimental studies that were applied to investigate the micromechanical behavior of asphalt material. The modeling work has employed finite element techniques to develop a microstructural model of heterogeneous asphalt materials. The model simulates the load transfer between aggregates using a micro-frame network scheme whereby the binder-aggregate system is replaced by an equivalent network of finite elements. The current work extended the model simulation to include nonlinear, softening behavior using damage mechanics theory. This concept developed a softening element that was capable of predicting the large inelastic response of asphalt materials. The formulation was implemented using the ABAQUS commercial FEA code. Model results for the overall sample response compared favorably with experimental data for indirect tension tests. Also, preliminary comparisons of sample micro- fracture/failure behaviors compared well with observed experimental photographic data. Additional experimental work included characterization studies of binder samples.

17. Key Words	18. Distribution Statement
Recycled Asphalt, Finite Element Modeling, Asphalt Microstructure, Numerical Simulation	No restrictions. This document is available to the public through the University of Rhode Island Transportation Center, 85 Briar Lane, Kingston, RI 02881

19. Security Classif. (of this report)	20. Security Classif. (of this page)	21. No. of Pages	22. Price
Unclassified	Unclassified	39	N/A

Form DOT F 1700.7 (8-72) Reproduction of completed page authorized (art. 5/94)

TABLE OF CONTENTS

List of Figures

ABSTRACT

This report describes the third year's research activities of a project dealing with the micromechanical behavior of asphalt materials. The project involved both theoretical/numerical modeling and experimental studies that were applied to investigate the micromechanical behavior of asphalt material. The modeling work has employed finite element techniques to develop a microstructural model of heterogeneous asphalt materials. The model simulates the load transfer between aggregates using a micro-frame network scheme whereby the binder-aggregate system is replaced by an equivalent network of finite elements. The current work extended the model simulation to include nonlinear, softening behavior using damage mechanics theory. This concept developed a softening element that was capable of predicting the large inelastic response of asphalt materials. The formulation was implemented using the ABAQUS commercial FEA code. Model results for the overall sample response compared favorably with experimental data for indirect tension tests. Also, preliminary comparisons of sample micro-fracture/failure behaviors compared favorably with observed experimental photographic data. Additional experimental work included characterization studies of binder samples.

1. INTRODUCTION

This report describes the third year's research activities of a project investigating the micromechanical behavior of asphalt materials. The project involved both theoretical/numerical modeling and experimental studies. These were applied to investigate the micromechanical behavior of asphalt material that included a percentage of reclaim products (RAP). Section 2 of the report represents the draft of a paper to be presented at the January 2003 meeting of the Transportation Research Board. Section 3 describes more recent work on visualization methods that have been used in the study, and section 4 briefly reviews some experimental binder characterization studies that provided particular material parameters for the modeling.

2. FINITE ELEMENT MICROMECHANICAL MODEL

2.1 Introduction

Asphalt is a complex heterogeneous material composed of aggregate, binder/cement, additives and void space. The load carrying behavior and resulting failure of such materials depends on many phenomena that occur at the aggregate/binder level. Thus the overall macro behavior is determined by the micromechanics within the cemented particulate system. Special additives and recycled asphalt product are also commonly used in pavement mixes, and this further complicates the material behavior by introducing several ageing effects such as hardening, chemical oxidation and binder micro-cracking. Because of the heterogeneous multiphase nature of asphalt material, it does not appear that traditional continuum mechanics theory will be able to predict important micro-behavior at the aggregate/binder level, and thus micromechanics modeling is needed. An understanding of the micromechanics offers the possibility to more accurately predict asphalt failure behavior and to relate such behavior to particular mix parameters such as binder properties and aggregate size, shape and gradation. The purpose of the present work is to develop a micromechanical model for asphalt concrete using a special finite element scheme incorporating damage mechanics concepts.

Over the past two decades, many studies have been investigating the micromechanical behavior of particulate, porous and heterogeneous materials. For example, studies on cemented particulate materials by Dvorkin et al. (1) and Zhu et al. (2) provide information on the basic load transfer between particles that are cemented together. Such studies provide details on the normal and tangential inter-particle load transfer, and would be fundamental in developing a micromechanical theory for load distribution and failure of such materials. Several recent applications of such contact-based micromechanical analysis for asphalt behavior have been reported by Chang and Gao (3), Cheung, et al. (4) and Zhu et al. (5). In a related study, Krishnan and Rao (6) used mixture theory and presented a multi-phase approach to explain air void reduction in asphalt materials under load.

Numerical modeling of cemented particulate materials has generally used both finite and discrete element methods. The discrete element method (DEM) analyzes particulate systems by modeling the translational and rotational behaviors of each particle using Newton's second law with appropriate inter-particle contact forces. Normally the scheme establishes an explicit, time-stepping procedure to determine each of the particle motions. DEM studies on cemented particulate materials include the work by Rothenburg, et al. (7), Chang and Meegoda (8), Trent and Margolin (9), Buttlar and You (10), Ullidtz (11) and Sadd et al. (12,13).

In regard to finite element modeling (FEM), Stankowski (14) applied standard FEM techniques to cemented particulate composites. Sepehr et al. (15) used an idealized finite element microstructural model to analyze the behavior of an asphalt pavement layer. A common finite element approach to simulate particulate and heterogeneous materials has used an *equivalent lattice network system* to represent the inter-particle load transfer behavior. This type of microstructural modeling has been used previously; Bazant, et al. (16), Mora (17), Sadd et al. (18) and Budhu, et al. (19). Along similar lines, Guddati, et al. (20) recently presented a random truss lattice model to simulate micro-damage in asphalt concrete and demonstrated some

interesting failure patterns in indirect tension test geometry. Birgisson et al. (21) used a displacement discontinuity boundary element approach to model asphalt mixtures. Bahia et al. (22) have also used finite elements to model the aggregate-binder response of asphalt materials, and Papagiannakis, et al. (23) have conducted similar studies for the viscoelastic response. Mustoe and Griffiths (24) developed a finite element model, which was equivalent to a particular discrete element approach. They pointed out that the FEM model has an advantage over the discrete element scheme for static problems.

This paper presents a numerical modeling scheme for asphalt concrete based on micromechanical simulation using the finite element method. The model first incorporates an equivalent lattice network approach whereby the local interaction between neighboring particles is modeled with a special frame-type finite element. The element stiffness matrix is constructed by considering the normal, tangential and rotation behaviors between cemented particles, and this is accomplished using an approximate elasticity solution within the cementation interface. The inelastic softening behavior exhibited by these materials is developed by incorporating a damage mechanics theory within the FEM model. Although this network approach is similar to other reported models, it is the element stiffness equation, which makes this work different from previous research. This theoretical formulation was then implemented into the commercial *ABAQUS* FEA code using user-defined elements. A series of model simulations of indirect tension tests (IDT) were conducted to investigate the effect of variation of specimen microstructure on the sample response. IDT samples were generated using a MATLAB material-generating code specially developed for this modeling effort. Simulation results of the overall sample behavior compared favorably with experimental results of actual asphalt samples. Additional comparisons were made of the evolving damage behavior within the IDT specimen, and numerical results gave reasonable predictions. Such a micromechanical model can provide important connections between asphalt material performance and details on the mix design.

2.2 Micromechanical Finite Element Model

As mentioned, bituminous asphalt can be described as a multi-phase material containing aggregate, binder cement (including mastic and fine particles) and air voids (see Figure 1). The

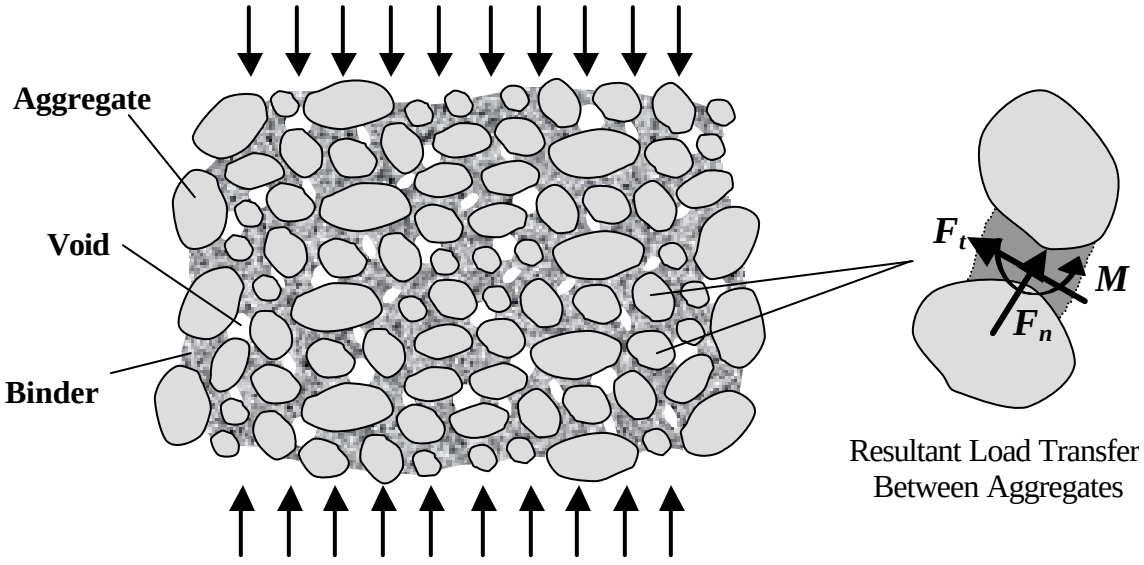

FIGURE 1 Multi-phase asphalt material.

load transfer between the aggregates plays a primary role in determining the load carrying capacity and failure of such complex materials. In order to develop a micromechanical model of this behavior, proper simulation of the load transfer between the aggregates must be accomplished. The aggregate material is normally much stiffer than the binder, and thus aggregates are taken as rigid particles. On the other hand, the binder cement is a compliant material with elastic, inelastic, and time-dependent behaviors. Additionally, binder behavior can also include hardening, debonding and micro-cracking, and these lead to many complicated failure mechanisms. In order to properly account for the load transfer between aggregates, it is assumed that there is an effective binder zone between neighboring particles. It is through this zone that the micro-mechanical load transfer occurs between each aggregate pair. This loading can be reduced to resultant normal and tangential forces and a moment as shown in Figure 1.

In order to model the inter-particle load transfer behavior, some simplifying assumptions must be made about allowable aggregate shape and the binder geometry. Studies on aggregate geometry have commonly quantified particle size, shape, angularity and texture. However, for the present modeling only size and shape will be considered. In general, asphalt concrete contains aggregate of very irregular geometry as shown in Figure 2(a). Our approach is to allow variable size and shape using an elliptical aggregate model as represented in Figure 2(b). The finite element model uses an *equivalent lattice network approach*, whereby the inter-particle load transfer is simulated by a network of specially created frame-type finite elements connected at particle centers as shown in Figure 2(c). From granular materials research, the material microstructure or *fabric* can be characterized to some extent by the *branch vector distribution*, which are the line segments from adjacent particle mass centers. Note that the proposed finite element network coincides with the branch vector distribution.

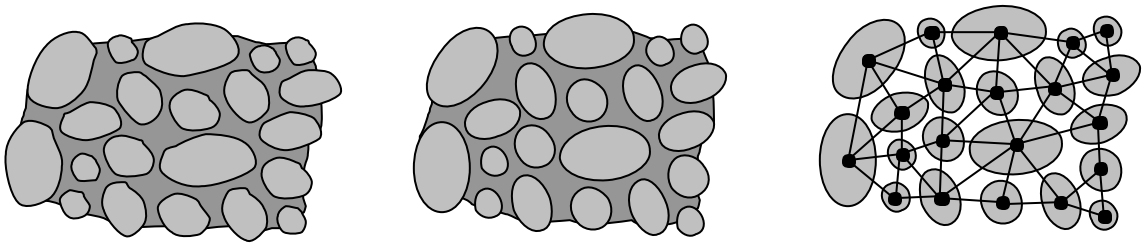

(a) Typical Asphalt Material (b) Model Asphalt System (c) Network Finite Element Model

FIGURE 2 Asphalt modeling concept.

The network model uses a specially developed, two-dimensional frame-type finite element to simulate the inter-particle load transfer. These two-noded elements have the usual three degrees-of-freedom (two displacements and a rotation) at each node and thus require a 6x6 stiffness matrix to relate nodal (aggregate) motions to the applied forces and moments. Thus the element equation is written as

$$\begin{bmatrix} K_{11} & K_{12} & K_{13} & K_{14} & K_{15} & K_{16} \\ . & K_{22} & K_{23} & K_{24} & K_{25} & K_{26} \\ . & . & K_{33} & K_{34} & K_{35} & K_{36} \\ . & . & . & K_{44} & K_{45} & K_{46} \\ . & . & . & . & K_{55} & K_{56} \\ . & . & . & . & . & K_{66} \end{bmatrix} \begin{Bmatrix} U_1 \\ V_1 \\ \theta_1 \\ U_2 \\ V_2 \\ \theta_2 \end{Bmatrix} = \begin{Bmatrix} F_{n1} \\ F_{t1} \\ M_1 \\ F_{n2} \\ F_{t2} \\ M_2 \end{Bmatrix} \quad (1)$$

where U_i, V_i and $?_i$ are the nodal displacements and rotations, and $F_{..}$ and $M_{.}$ are the nodal forces. The usual scheme of using bar and/or beam elements to determine the stiffness terms is not appropriate for the current modeling, and therefore these terms were determined using an approximate elasticity solution from Dvorkin et al. (1) for the stress distribution in a cement layer between two particles. We use the special case where the particle material stiffness is much greater than that of the cement layer, and thus the particles are assumed to be rigid. Dvorkin has shown that effects of non-uniform cement thickness for each binder element are generally small, and so the analytical solution with average cement thickness for each binder element was used. The two-dimensional model geometry is shown in Figure 3. Note that we are allowing arbitrary non-symmetric cementation, and thus the finite element line will not

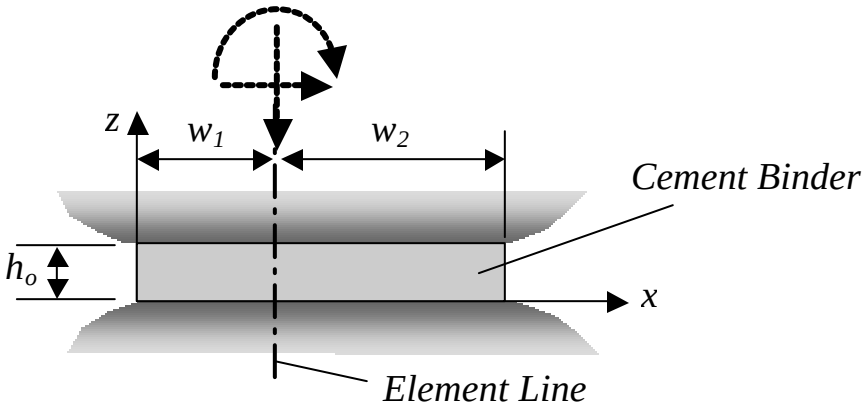

FIGURE 3 Cement binder between two adjacent particles.

necessarily pass through the center of the binder material. Thus in general, $w = w_1 + w_2$, but $w_1 \neq w_2 \neq w/2$, and an eccentricity variable may be defined by $e = (w_2 - w_1)/2$.

The stresses σ_x, σ_z and τ_{xz} within the cementation layer can be calculated for particular relative particle motion cases involving normal, tangential and rotational deformation. These stresses can then be integrated to determine the total load transfer within the cement binder, thus leading to the calculation of the various stiffness terms needed in the element equation. The details of this process have been previously reported by Sadd and Dai (25), and the final result is given by

$$[K] = \begin{bmatrix} K_{nn} & 0 & K_{nn}e & -K_{nn} & 0 & -K_{nn}e \\ \cdot & K_{tt} & K_{tt}r_1 & 0 & -K_{tt} & K_{tt}r_2 \\ \cdot & \cdot & K_{tt}r_1^2 + \frac{K_{nn}}{3}\left(w_2^2 - w_1w_2 + w_1^2\right) & -K_{nn}e & -K_{tt}r_1 & K_{tt}r_1r_2 - \frac{K_{nn}}{3}\left(w_2^2 - w_1w_2 + w_1^2\right) \\ \cdot & \cdot & \cdot & K_{nn} & 0 & K_{nn}e \\ \cdot & \cdot & \cdot & \cdot & K_{tt} & -K_{tt}r_2 \\ \cdot & \cdot & \cdot & \cdot & \cdot & K_{tt}r_2^2 + \frac{K_{nn}}{3}\left(w_2^2 - w_1w_2 + w_1^2\right) \end{bmatrix} \quad (2)$$

where $K_{nn} = (\lambda+2\mu)w/h_o$, $K_{tt} = \mu w/h_o$, λ and μ are the usual elastic moduli, h_o is the average cementation thickness, r_1 and r_2 are the radial dimensions from each aggregate center to the cementation boundary, w_1 and w_2 are cementation widths, and $e = (w_2 - w_1)/2$. Each binder element stiffness matrix is significantly different depending on two-particle layout and size and binder geometry. This procedure establishes the elastic stiffness matrix, and it is clearly a function of the micromechanical material variables including particle size and shape and cementation geometry and moduli.

2.3 Damage Mechanics Model

In order to simulate the inelastic and softening behaviors observed in asphalt materials, a damage mechanics approach was applied within the inter-particle cementation model. Although

work on such a damage model has been previously reported by Zhong and Chang (26), the approach by Ishikawa, Yoshikawa and Tanabe (27) was found to be more useful for our finite element model. The theory was originally developed for concrete materials whereby the internal micro-cracks within the matrix cement and around the aggregates are modeled as a continuous defect field. Inelastic behavior is thus developed by the growth of damage within the material with increasing loading. A *damage tensor* $[\Omega]$ is defined by considering the reduction of the effective area of load transfer within the continuum. The total strain field is defined as the sum of the elastic and damage strains

$$\{e\} = \{e_e\} + \{e_f\} \tag{3}$$

and thus the elastic constitutive relationship can be expressed as

$$\{s\} = [D_o]\{e_e\} = [D_o]\{e - e_f\} \tag{4}$$

where $[D_o]$ is initial elastic stiffness matrix.

The damage strain represents the difference between the total and elastic strains and can be written as

$$\{e_f\} = \{e\} - \{e_e\} = [D_o]^{-1}[\Omega][D_o]\{e\} \tag{5}$$

This leads to the development of a damage stiffness matrix $[D_s]$ defined by

$$\{s\} = ([I] - [\Omega])[D_o]\{e\} = [D_s]\{e\} \tag{6}$$

The damage stiffness matrix can be obtained from the initial elastic stiffness matrix

$$[D_s] = ([I] - [\Omega])[D_0] \tag{7}$$

In order to characterize the nonlinear damage behavior of asphalt concrete, a particular Weibull distribution function is chosen to describe the evolution of the defect field within the binder cement. Such forms have been used before and for the uniaxial hardening response, the constitutive relation is taken as

$$s = s_0(1-e^{-b(e/e_0)}) \Rightarrow \frac{\partial s}{\partial e} = D_0 e^{-b(e/e_0)} \tag{8}$$

where the material parameters e_0 and b are related to the softening strain and damage evolution rate respectively, s_0 is the material strength, and $D_0 = s_0 b/e_0$ is the initial elastic stiffness. Using the damage stiffness definition from relationship (7), the uniaxial damage stiffness D_s and the damage scalar Ω become

$$D_s = (1-\Omega) D_0 = D_0 e^{-b(e/e_0)}, \text{ where } \Omega = 1 - e^{-b(e/e_0)} \tag{9}$$

In this model, the critical damage scalar Ω_c and critical strength s_c are expressed as

$$\Omega_c = 1 - e^{-b}, \text{ and } s_c = s_0(1-e^{-b}) \tag{10}$$

Note that the critical value of the damage scalar Ω_c could be less than 1 for asphalt concrete. Once the damage scalar reaches Ω_c, the material point will gradually lose its stiffness.

After critical strength the softening behavior is taken as

$$s = s_0(1-e^{-b})e^{m(1-e/e_0)} \Rightarrow \frac{\partial s}{\partial e} = -\frac{D_0 m}{b}(1-e^{-b})e^{m(1-e/e_0)} \tag{11}$$

where m is a material parameter related to the softening rate. And the corresponding damage softening stiffness D_s and the virtual damage scalar Ω become

$$D_s = (1-\Omega) D_0 = -\frac{D_0 m}{b}(1-e^{-b})e^{m(1-e/e_0)}, \text{ where } \Omega = 1 + \frac{m}{b}(1-e^{-b})e^{m(1-e/e_0)} \tag{12}$$

The uniaxial stress-strain response corresponding to this particular constitutive model is shown in Fig. 4 for the case of $\varepsilon_o = 0.3$, $b = 5$ and $m = 1$.

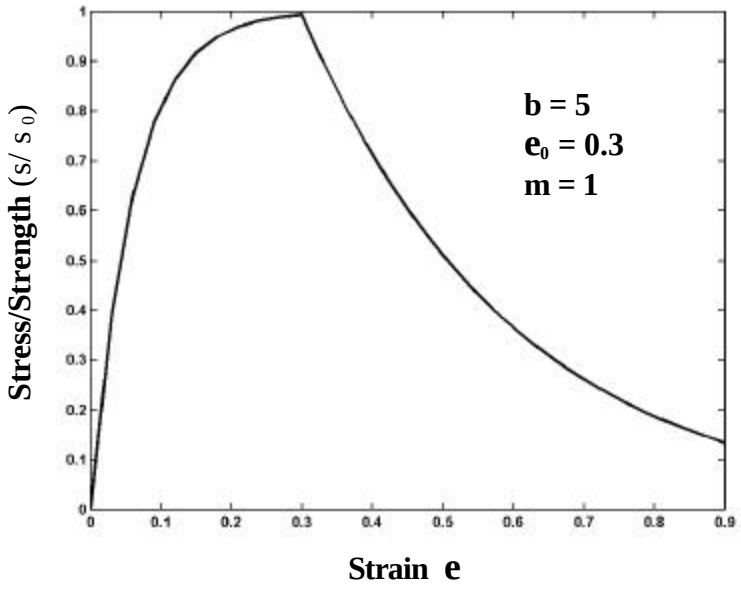

FIGURE 4 Uniaxial stress-strain response for damage model.

This damage-modeling scheme was incorporated into the finite element network model by modifying the micro-frame element stiffness matrix given in equation (2). Using the uniaxial relation (9), the normal and tangential damage stiffness terms for the hardening behavior can be separately written as

$$\left(K_{nn}\right)_s = K_{nn} e^{-b(\Delta u_n / \Delta U_n)}, \left(K_{tt}\right)_s = K_{tt} e^{-b(\Delta u_t / \Delta U_t)} \tag{13}$$

and using equation (12) the corresponding normal and tangential damage softening stiffnesses are given as

$$\left(K_{nn}\right)_s = -(K_{nn} m / b)(1 - e^{-b}) e^{m(1-\Delta u_n / \Delta U_n)}$$

$$\left(K_{tt}\right)_s = -(K_{tt} m / b)(1 - e^{-b}) e^{m(1-\Delta u_t / \Delta U_t)} \tag{14}$$

where Δu_n and Δu_t are the normal and tangential accumulated relative displacements and ΔU_n and ΔU_t are the normal and tangential displacement softening criteria. Thus the micro-

frame element damage stiffness matrix $[K_s]$ is constructed from equation (2) by replacing K_{nn} and K_{tt} with $(K_{nn})_s$ and $(K_{tt})_s$.

The initiation of binder softening behavior for tension, compression and shear is governed by softening criteria based on accumulated relative displacements between particle pairs. A simple and convenient scheme to determine the softening criteria is based on using the dimensions of the inter-particle binder geometry in the form

$$\begin{aligned} \Delta U_n^{(t)} &= c_{nt} h_o \\ \Delta U_n^{(c)} &= c_{nc} h_o \\ \Delta U_t &= c_{tt} w \end{aligned} \tag{15}$$

where c_{nt}, c_{nc}, c_{tt} represent tension, compression and shear *softening factors*. These material constants correspond to the critical strength and can be determined from experimental data. Since the cementation geometry h_o and w will in general be different for each particle pair, it is expected that each element will have different softening criteria related to its local microstructure.

This model binder damage behavior is a result of the material's defects including micro-cracks, voids and joints. Additional defects in the multiphase asphalt system could include interface cracks between the aggregates and binder, commonly caused by settlement of aggregate during compaction. As external loading is increased, existing micro-cracks coalesce to form finite cracks thus leading to interior failure of the binder or interfacial debonding with the aggregates. When the two-particle binder element is subjected to tension and/or shear force, the element was allowed to soften (interfacial damage) after the loading exceeded appropriate bond strength. Since tension and shear behaviors are coupled, the binder element would lose all its tension and shear stiffness after the element has interfacially softened. Compressional damage softening is viewed as the Mode-II fracture behavior of micro-cracks inclined to the loading direction.

For compressional behavior between particle pairs, the cementation spacing will decrease with load increment. Eventually, softening behavior will be initiated and the total element stiffness will significantly decrease. This will lead to the closing of the cementation gap when $\Delta u_n^{(c)} = h_0$, thus creating contact between the aggregates. At this point the element normal stiffness must be modified to account for this change of physics. The aggregate-to-aggregate stiffness would be significantly higher than the cementation elastic stiffness and currently the model uses a contact stiffness three orders of magnitude larger than the elastic stiffness.

This softening modeling scheme was incorporated into the ABAQUS finite element code using the nonlinear User Defined Element (UEL) subroutine. UEL subroutine would determine the compression and tension force in each element and perform the required damage calculations in the normal and tangential directions. In the ABAQUS analysis, displacement control boundary conditions were employed and the Modified Riks method was used in order to provide a more stable solution scheme. Also, because aggregate (nodal) displacements became sizeable, the mesh geometry was updated during each load increment.

2.4 Indirect Tension Test Simulations

The indirect tension test (IDT) involves the compressional loading of a cylindrical specimen along its diameter, and is commonly used to determine the tensile or splitting strength of bituminous materials. Since this test encompasses softening failure and fracture damage, it appears to be well suited for micromechanical simulation using our damage model. Under the assumption of uniform loading through the thickness, a two-dimensional circular cross-section may be used for numerical simulation. Several numerical IDT samples have been created using a MATLAB material generating code specially developed for this modeling effort. The generating code provides a convenient numerical routine to spatially distribute particles of general elliptical size and to distribute binder cement between adjacent aggregate pairs. The code allows user control over the details of the generated microstructure or fabric, and this

establishes the nature and connectivity of the finite element mesh. Finally the code generates the required input files needed for the finite element simulation program. Details on this material generating code have been previously given (25). Figure 5 illustrates three particular models that have been developed for simulation. All models have approximately the same overall diameter of 101mm (4in) and thickness of 63mm (2.5in), and this was chosen to allow comparison with previously collected experimental test data on standard 4in samples. Model 1 had 65 particles (in four particle size groupings) resulting in 201 finite elements. Model 2 used a variable aggregate size distribution of 71 circular particles in groupings of 14, 11, 7 and 4mm to

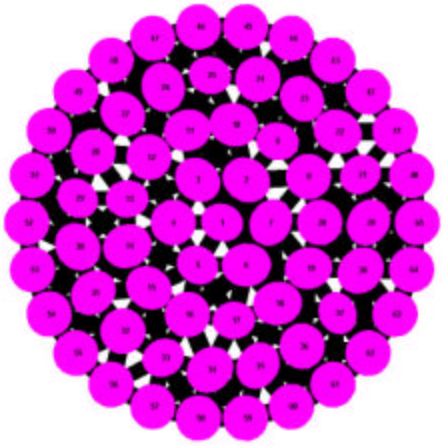

Model 1
65 particles, 201 elements

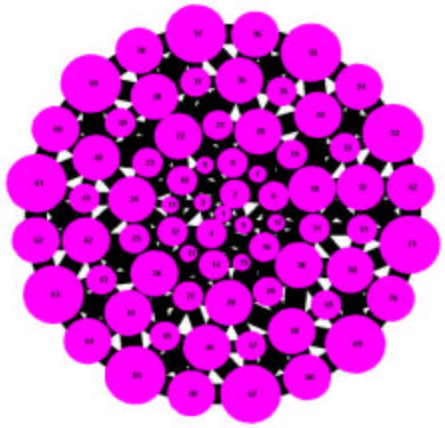

Model 2
71 particles, 232 elements

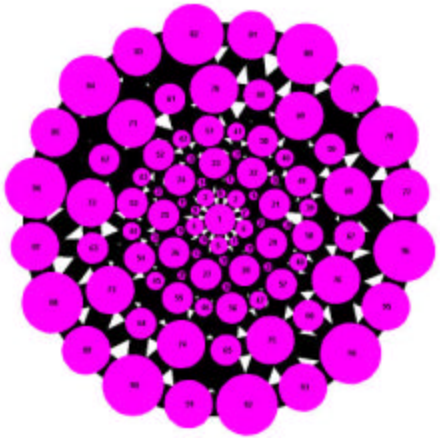

Model 3
96 particles, 286 elements

FIGURE 5 IDT microstructural models.

approximate an actual sample gradation curve. This resulted in 232 model elements. Model 3 had 96 particles from groups of 14, 11, 7, 4 and 2mm and this gave 286 elements. Thus each of the three generic models had somewhat different internal microstructure, and further differences were created through variation in the binder moduli and damage parameters. Model boundary conditions constrain both horizontal and vertical displacements of the bottom pair of aggregates, while the top particle pair accepts the applied vertical displacement loading.

A series of numerical IDT simulations were conducted for each of the three models using different values of binder softening factors. Figure 6 shows the IDT sample simulation response of vertical load versus displacement for Model 1 using three different compression-softening factors. Since each case had identical elastic and hardening parameters, the initial hardening responses are essentially the same. However, as the compression-softening factor is increased, less softening behavior is generated and these cases will produce a higher maximum load as shown. Similar results have been found for Models 2 and 3. It is noted that Model 3 with the higher percentage of fine material gives a slightly stiffer response in comparison to Model 2.

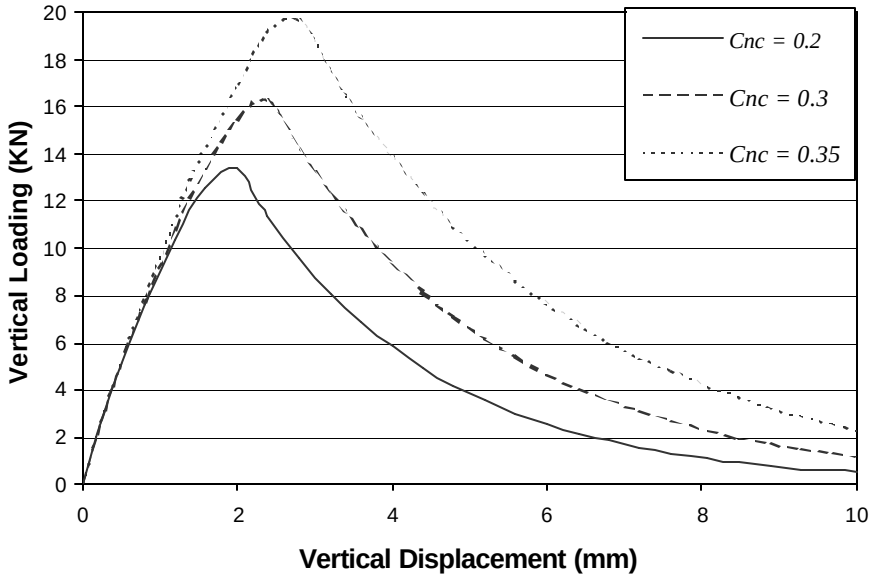

FIGURE 6 IDT simulations of Model 1 for different compression softening factors. Model parameters: E = 71.5MPa, v = 0.3, b = 2, m = 0.8, c_{tt} = 0.2, c_{nt} = 0.2.

Numerical simulation results for these three models have also been compared with experimental data for a particular asphalt mix containing 30% of recycled product. Figure 7 shows the model comparisons with data from three IDT tests. It is evident that the simulations compare favorably with the data, thus indicating that the softening damage model can be used to predict such behavior.

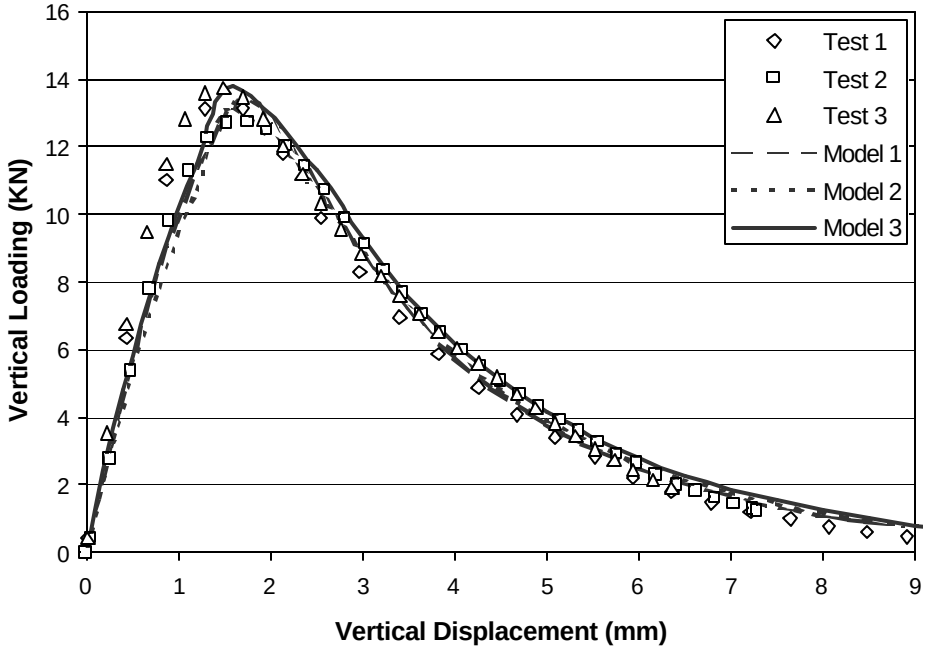

FIGURE 7 Comparison of IDT model simulations with experimental data.
Model 1 parameters: E = 71.5MPa, ν = 0.3, b = 2, m = 0.8, c_{nc} = 0.2, c_{tt} = 0.2, c_{nt} = 0.2.
Model 2 and 3 parameters: E = 63.5MPa, ν = 0.3, b = 2, m = 0.8, c_{nc} = 0.2, c_{tt} = 0.2, c_{nt} = 0.2.

In order to investigate the nature of the microstructural softening/damage processes within an IDT sample, a special series of numerical and experimental tests were conducted. The simulations involved the three models previously shown in Figure 5. The model assumes that there exists a continuous distribution of defects in the binder material. This defect field is taken to grow with the material deformation, and this results in a softening response of particular elements in the FEM network. As per equations (13) and (14), this softening behavior can affect the compression, tension and shear behavior of the element. As previously mentioned, in asphalt

material this evolving damage process involves the growth of micro-cracks to form macro-cracking and/or aggregate debonding. Each of the three models was subjected to incremental loading, and during this process all elements within the model were monitored for softening behavior. The element softening evolution and load-displacement response for each model are shown in Figures 8, 9 and 10. For each model, the initial onset of sample loading is shown in Figure (a) and this also indicates the initial tension and compression behavior within the finite element network. It was found that the largest compressional behavior occurred in vertical elements near the loaded centerline, while horizontal elements in this region perpendicular to the loading direction had the greatest tension loads. Later loading steps are shown in Figures (b), (c) and (d), and the location of these loading steps for each model are illustrated on the overall sample load-displacement plot. Early softening elements at loading step (b) did not significantly affect the stiffness, and models had nonlinear hardening behavior. Step (c) just past the model critical strength, generated small softening behavior, while step (d) had extensive softening as reflected in the large number of softening elements. It is observed that the evolution of damage occurs in the central portions of the model sample where the element loadings are the greatest. Preliminary photographic data from an actual IDT test was collected on the behavior of the surface aggregates and binder damage patterns. One particular photograph is shown in Figure 11, which illustrates the total softening (fracture) behavior along an irregular path through the binder material. The damage simulation results in Figures 8-10 qualitatively agree with the results shown in the photograph. Further work is needed to develop a relation between the damage growth and how it will specifically lead to binder fracture.

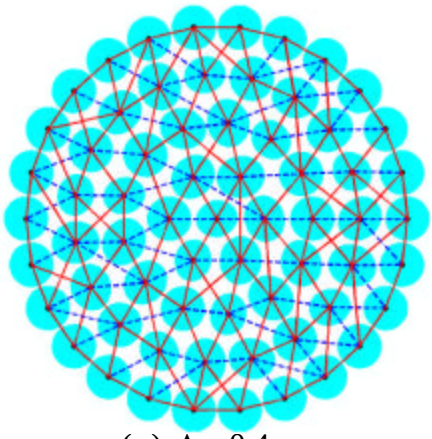

$(a)\ \Delta = 0.4mm$

Solid Lines - Compression Elements

Dashed Lines - Tension Elements

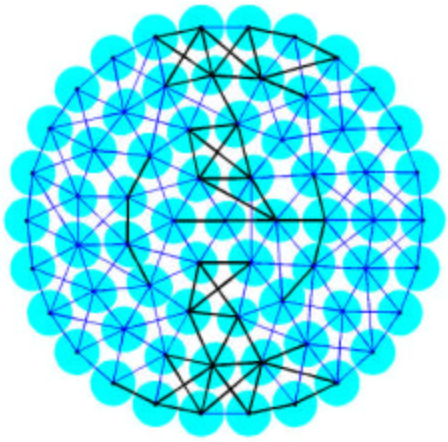

$(b)\ \Delta = 1.0mm$

Darkened Lines Indicate Softening Elements

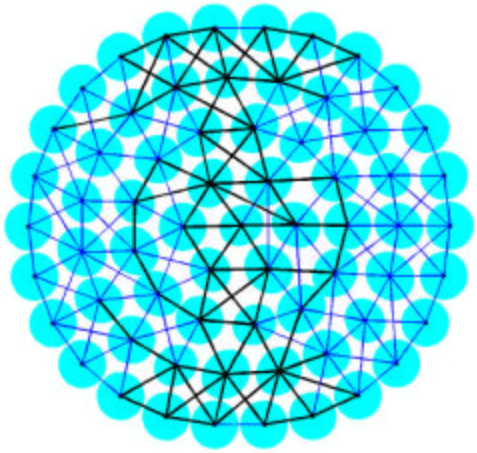

$(c)\ \Delta = 2.5mm$

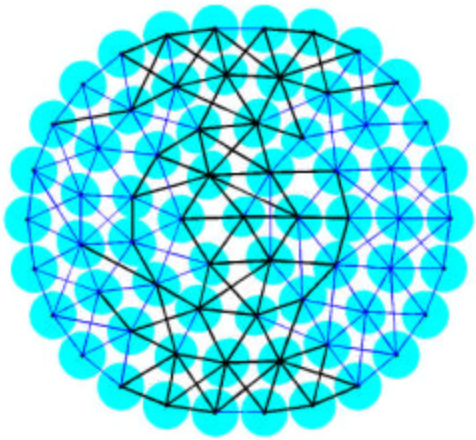

$(d)\ \Delta = 4.0mm$

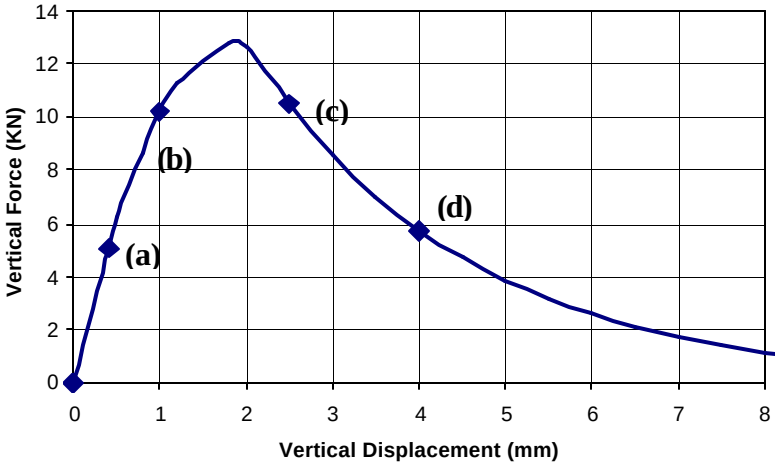

FIGURE 8 Model 1 softening element evolution and load vs displacement curve in IDT simulation.
Model 1 parameters: E = 71.5MPa, v = 0.3, b = 2, m = 0.8, c_{nc} = 0.2, c_{tt} = 0.2, c_{nt} = 0.2.

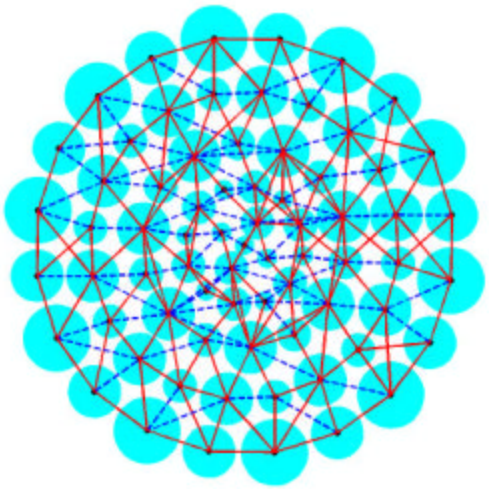

$(a)\ \Delta = 0.4mm$

Solid Lines - Compression Elements
Dashed Lines - Tension Elements

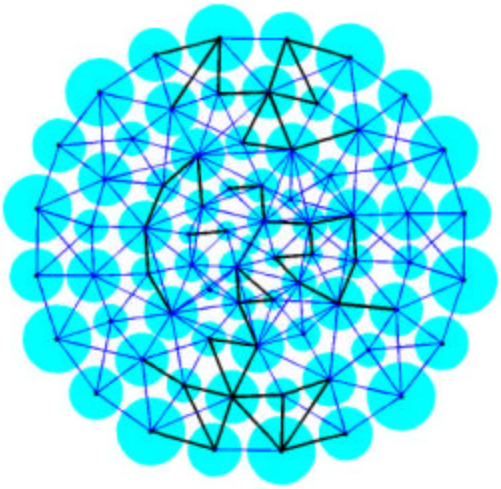

$(b)\ \Delta = 1.0mm$

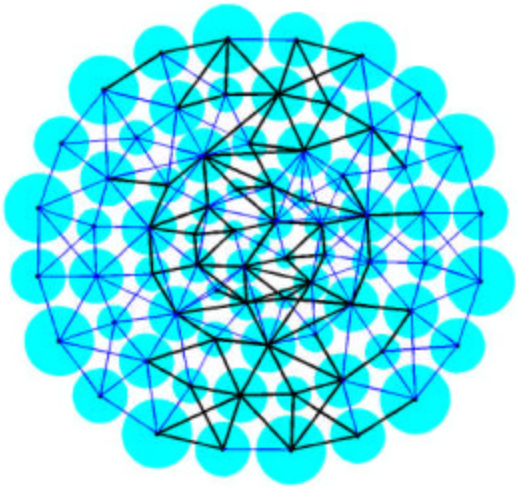

$(c)\ \Delta = 2.5mm$

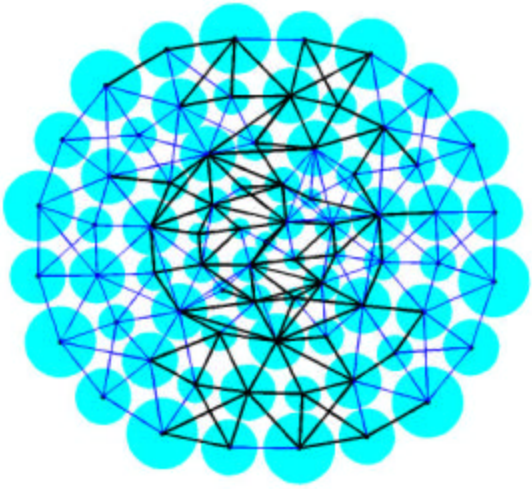

$(d)\ \Delta = 6.0mm$

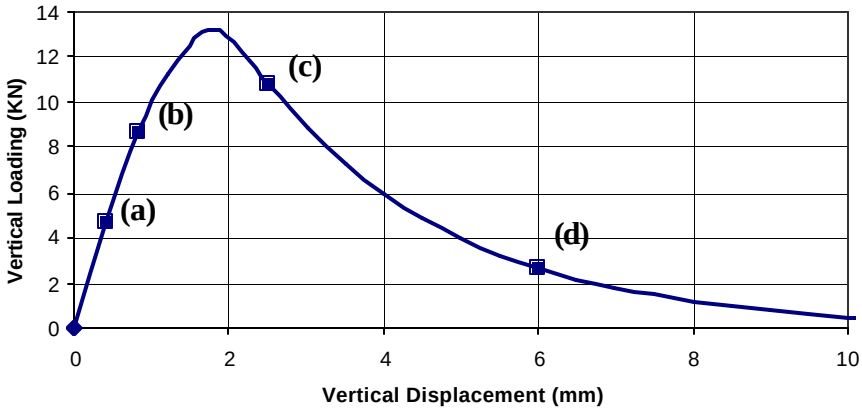

FIGURE 9 Model 2 softening element evolution and load vs displacement curve in IDT simulation. Model 2 parameters: E = 63.5MPa, v = 0.3, b = 2, m = 0.8, c_{nc} = 0.2, c_{tt} = 0.2, c_{nt} = 0.2.

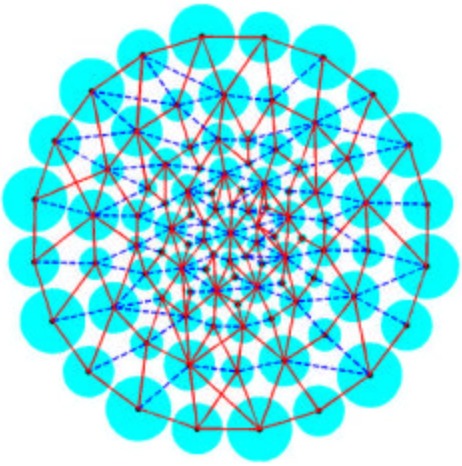

$(a)\ \Delta = 0.4mm$

Solid Lines - Compression Elements

Dashed Lines - Tension Elements

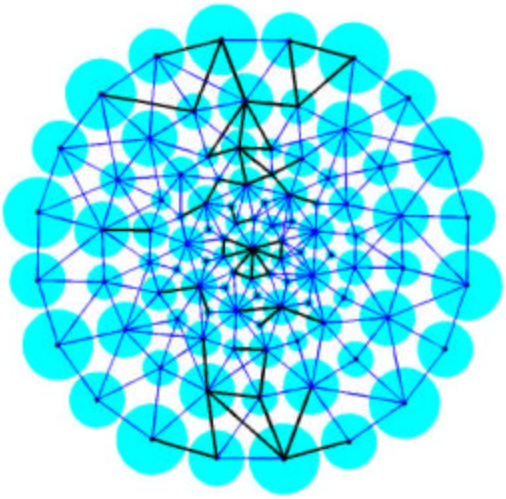

$(b)\ \Delta = 1.0mm$

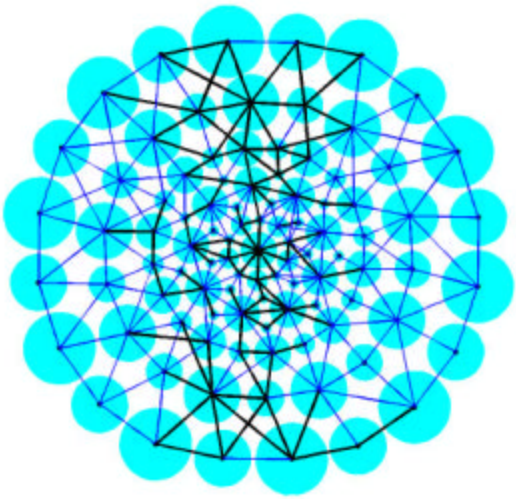

$(c)\ \Delta = 2.5mm$

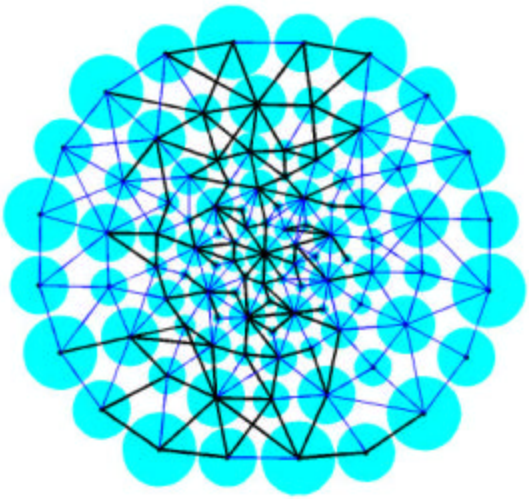

$(d)\ \Delta = 6.0mm$

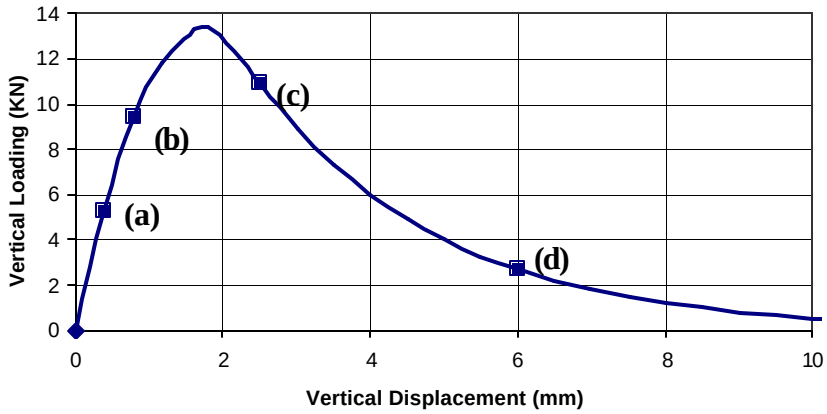

FIGURE 10 Model 3 softening element evolution and load vs displacement curve in IDT simulation. Model 3 parameters: E = 63.5MPa, v = 0.3, b = 2, m = 0.8, c_{nc} = 0.2, c_{tt} = 0.2, c_{nt} = 0.2.

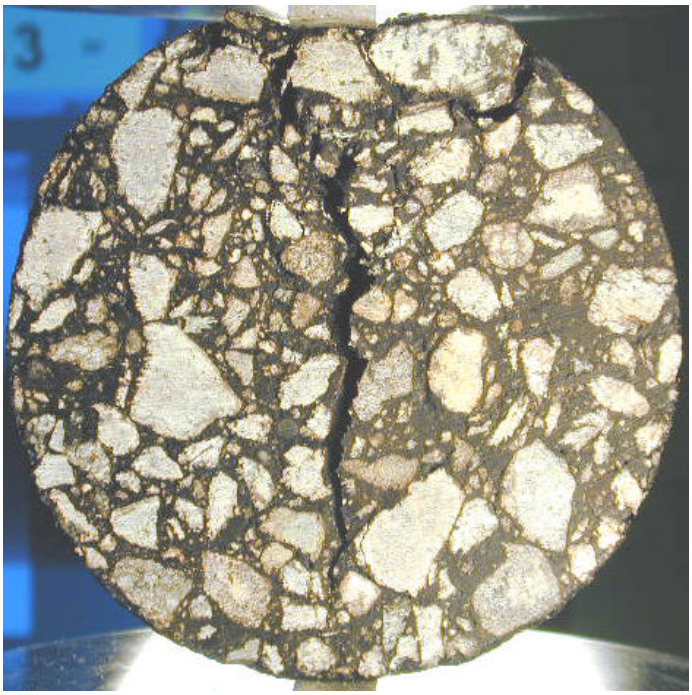

FIGURE 11 Typical failure geometry in an actual IDT sample.

3. VISUALIZATION AND DIGITAL MICROSTRUCTURE RECOGNITION STUDIES

This section describes our initial efforts in using digital microstructure recognition (DMR) to investigate asphalt behavior. Scanned surface section images of an indirect tension (IDT) specimen have been used in both experimental and modeling studies. Video images have been used to study the actual failure patterns under loading, and image analysis has been used on the initial microstructure to create a model for computer simulation.

3.1 IDT Experimental Testing Using Visualization Techniques

The experimental effort has used video imaging of real time asphalt material behavior to investigate the damage evolution and aggregate motions of an IDT sample. The samples had a diameter of 100 mm and thickness of 63 mm and were prepared with 30% RAP content through the Marshal compaction method. The details of the mix design and specimen preparation were identical to that followed for IDT testing outlined in the second year report Sadd, et.al. (28).

After compaction, the sample was sliced to a thickness of 25 mm in order to expose the aggregates for easy visualization. The 25 mm thickness was chosen since it was larger than the largest aggregate size (19 mm) in the mix. The front face of the sample is shown in Figure 12.

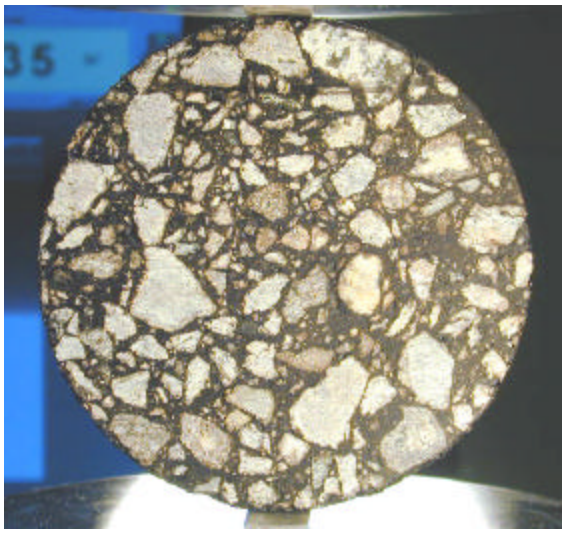

Figure 12. IDT sample microstructure.

The specimen was then tested under indirect tension and the real time sample deformation and damage evolution was photographed with a 2 mega pixel digital camera at the rate of one picture every 600 milliseconds. The load-deflection response of this sample is shown in Figure 13, and the real-time sequence of damage evolution and growth is shown in Figure 14. The sequence of the photographs is from left to right and the load at which the photograph was taken in shown in the upper right corner. These loading points are also indicated on Figure 13. It can be observed from the figure that the first appearance of damage in the form of cracks is visible in the fourth picture corresponding to a load value of 2940 N, which is the first photograph past reaching the peak load. The crack grows with further loading and finally splits the sample along the loaded diameter. It should be observed that the crack path progresses around the aggregates.

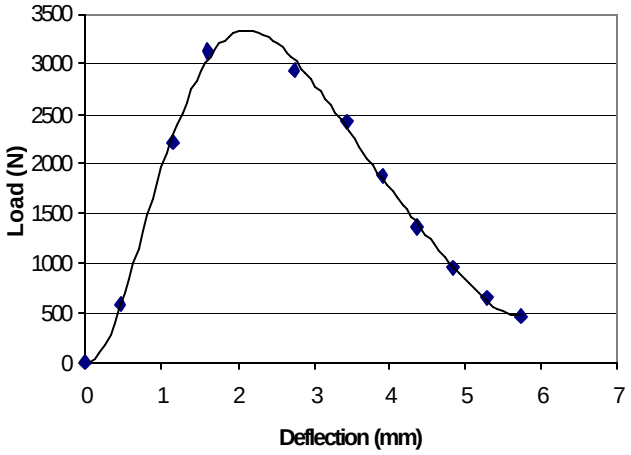

Figure 13. Load-deflection response of IDT sample used in real-time visualization of damage. The diamond points were obtained from the photographs.

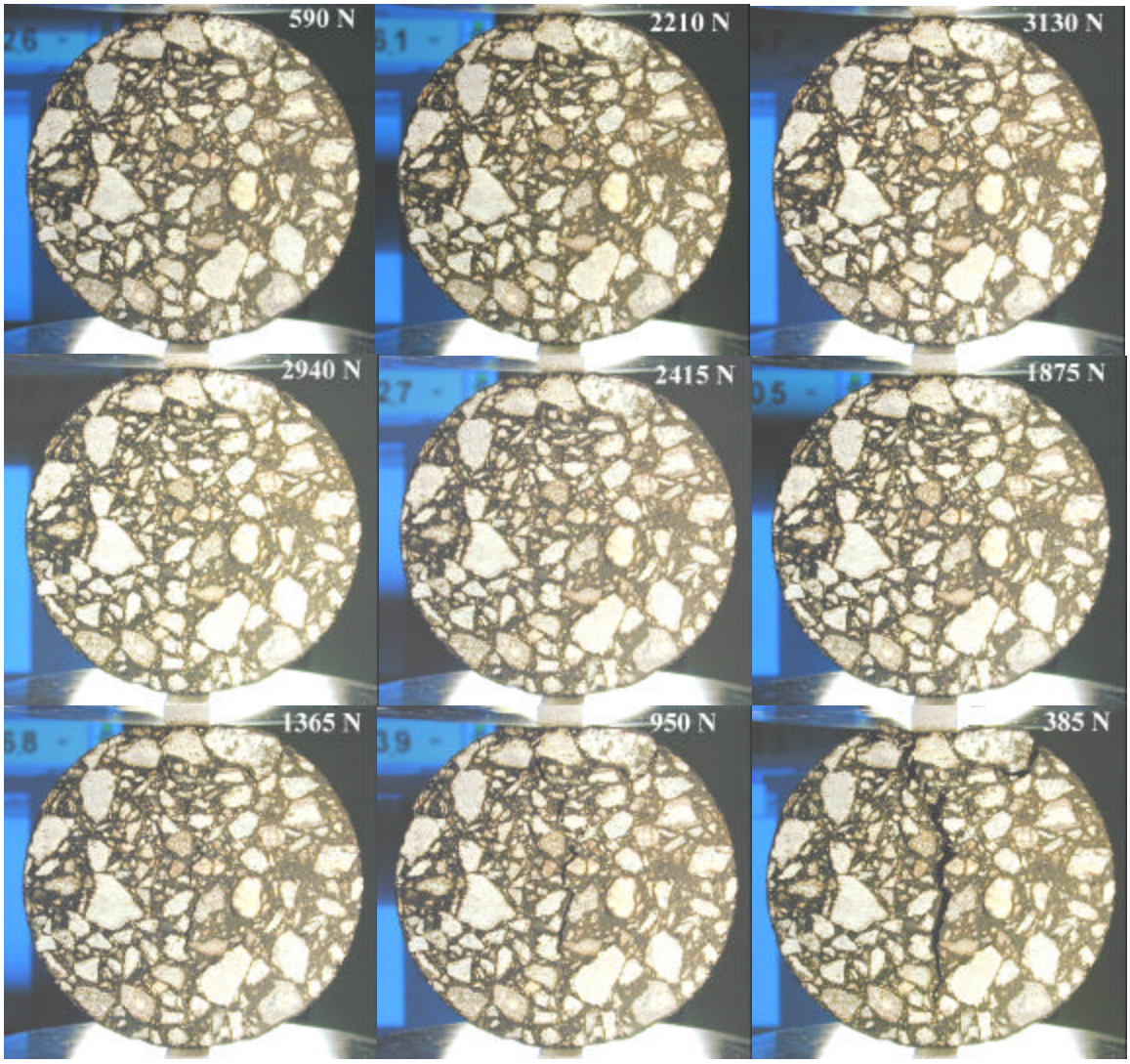

Figure 14. Real-time damage evolution in asphalt sample under indirect tension.

3.2 Visualization Techniques for IDT Model Generation and Simulation

Model Generation: Aggregate Extraction and Elliptical Least Square Fitting

Image processing was applied to the sectioned sample shown in Figure 12. In order to capture the real asphalt concrete microstructure, the MATLAB Imaging Toolbox, DIPimage Toolbox (29) and Adobe Photoshop were used. A least squares, ellipse-fitting algorithm was then incorporated to determine the "best" ellipse to represent each irregular aggregate geometry. A summary of these steps are shown in Figure 15.

The RGB image of the sectioned specimen was first obtained with a digital camera. This image was then converted to grayscale using Adobe Photoshop software as shown in Figure 15(a). Every pixel of a grayscale image has a brightness value ranging from 0 (black) to 255 (white). Grayscale aggregate images were then digitally sieved and least square fitted with an ellipse using ImagePro and EllipFit codes developed within MATLAB. The sequential steps in this process are:

Step 1. A grayscale threshold was applied to convert the original images to a binary (black and white) image, with white signifying the aggregates and black being the combination of binder, air void and aggregate fines (see Figure 15(b)). The image size 102×102 mm was digitized to 784×784 pixels, and this results in a 0.13 mm/pixel grid.

Step 2. Segmentation techniques were applied to the binary image to ensure that neighboring aggregate pixels did not artificially connect together shown as Figure 15(b). Digitally sieved aggregates with pixel sizes larger than sieving size 1mm (50 pixels) are shown in Figure 15(c).

Step 3. Each sieved aggregate was then labeled and selected it as separate image. The edge pixels of each aggregate were extracted, and the coordinates of these pixels were stored in an array for the ellipse fitting.

Step 4. Sieved aggregates were then fitted with the best ellipse using a new efficient direct least squares fitting method presented by Fitzgibbon (30). The fitting ellipse was then generated with the EllipFit code as shown in Figure 15(d), and its geometry (center coordinates and orientation) were stored for the computation model generation and simulation.

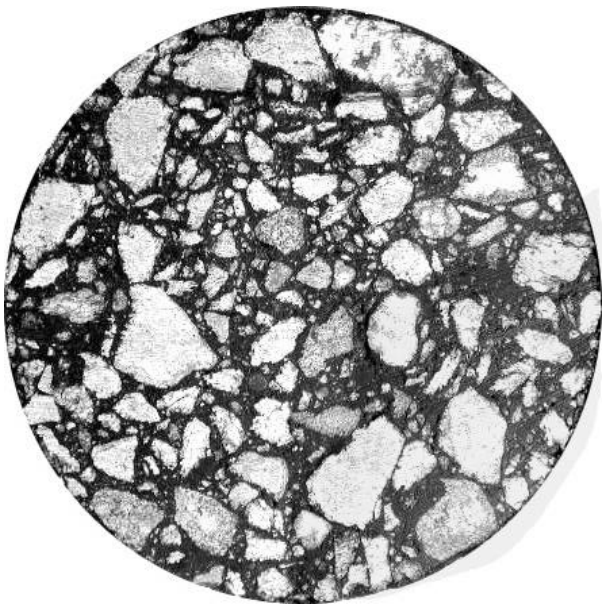

(a) Grayscale image

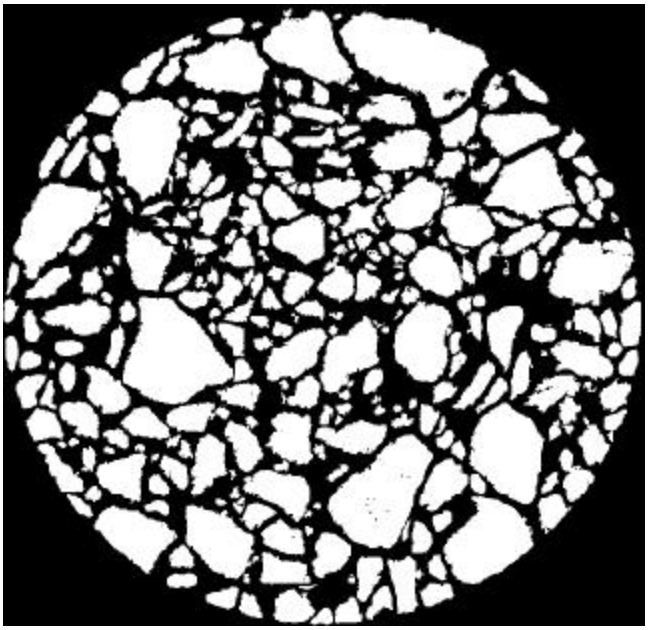

(b) Binary image with segmentation technique

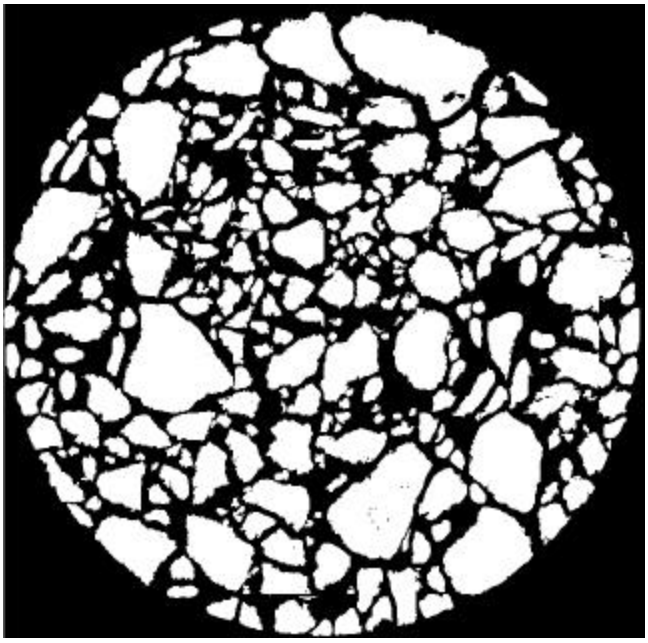

(c) Sieving aggregate (D>1mm)

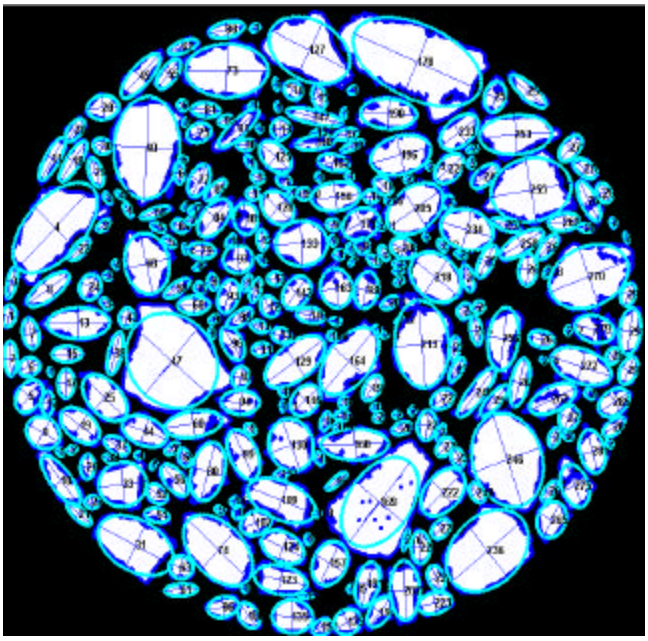

(d) Least squares ellipse fitting

Figure 15. Image processing and aggregate least squares ellipse fitting.

Model Generation and Simulation

Based on the ellipse parameters obtained from the previous image analysis, a computation model was generated using MATLAB as shown in Figure 16(a). Neighboring ellipses were maximally filled with cement binder as illustrated in Figure 17. The cement binder is symmetrical about the branch vector and completely fills the area between the two ellipse axes perpendicular to the branch vector. For this computational model, the porosity was approximately 4% and the sieved aggregate percentage is 62.5%. For IDT simulation, a special contact boundary condition was imposed on aggregates in contact with the top and bottom loading plates shown as figure 16(a). The normal contact behavior was simulated by using very stiff elastic finite elements, and a small sliding displacement was allowed between the contact aggregates and the bearing plates to model frictional behavior. The *x*- and *y*-displacements of the bottom plate and *x*-displacement of top plate were fixed. Sample loading was achieved by incrementing the *y*-displacement of the top plate. The overall dimensions of the model sample were the same as those of the experimental specimen previously given. The model material parameters were chosen as E = 43.5 Mpa, u = 0.3, b =2 and m = 1.2, and softening factors of $c_{nc} = 0.2,\ c_{nt} = 0.1,\ c_{tt} = 0.1.$

Figure 16 illustrates the model simulation results. Figures (a)-(d) show the element softening evolution for four different loading steps indicated by the sample vertical displacement Δ. These loading steps are illustrated on the overall load-displacement curve by the square points. Darkened lines indicate softening elements. The early loading step (a) did not significantly affect the model stiffness, whereas the later steps (b)-(d) produced considerable softening behavior with more softening elements. It is observed that the evolution of softening damage primarily occurs in the central portions of the model sample where the element loading is the largest. The overall load-displacement response of the model is also compared with experimental test data, and simulation results compare favorably with the data.

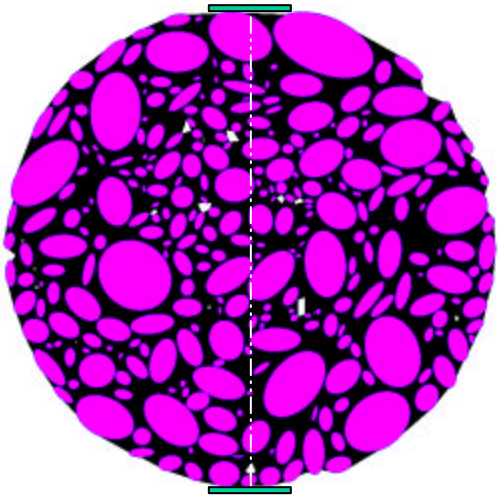

Imaging Computation Model
Porosity ≈ 4%

$(a)\ \Delta = 0.5mm$

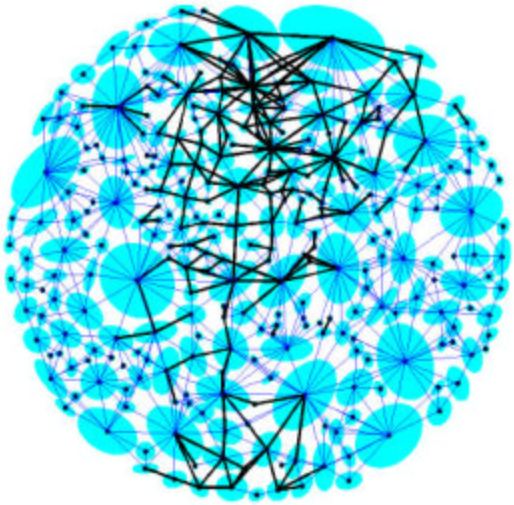

$(b)\ \Delta = 2mm$

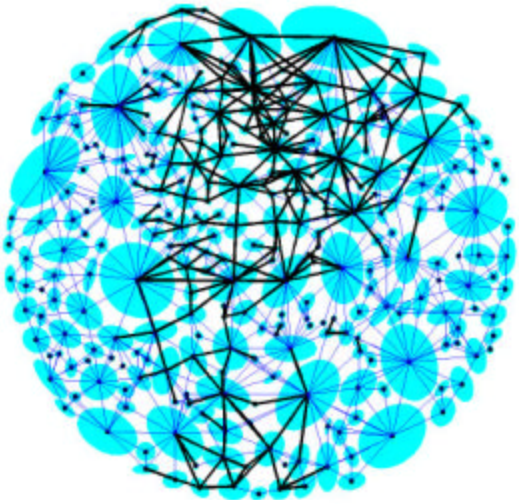

$(c)\ \Delta = 3mm$

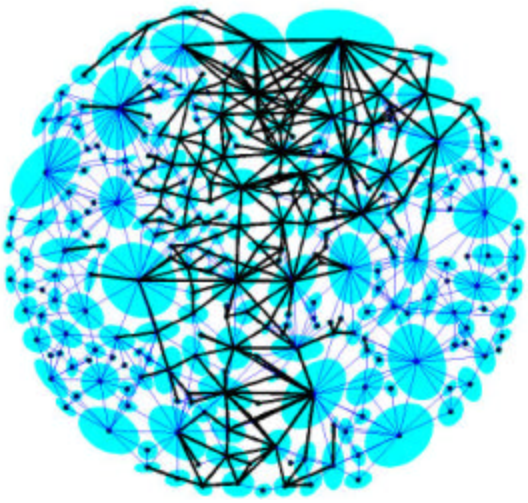

$(d)\ \Delta = 4mm$

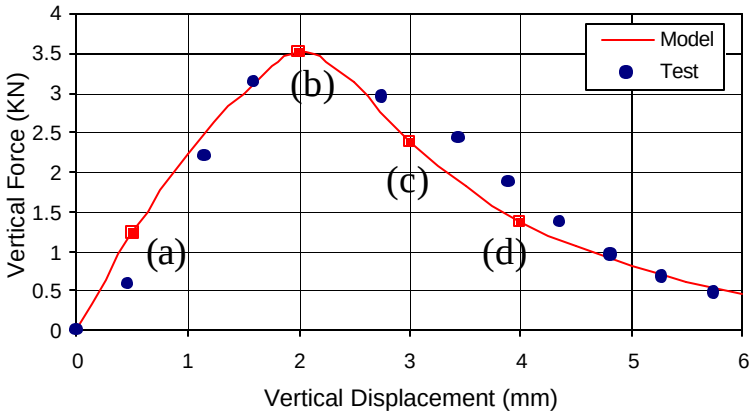

Figure 16. Softening element pattern and load vs displacement curve in IDT simulation

Model parameters: E = 47.5MPa, v = 0.3, b = 2, m = 1.2, c_{nc} = 0.2, c_{nt} = 0.1, c_{tt} = 0.1.

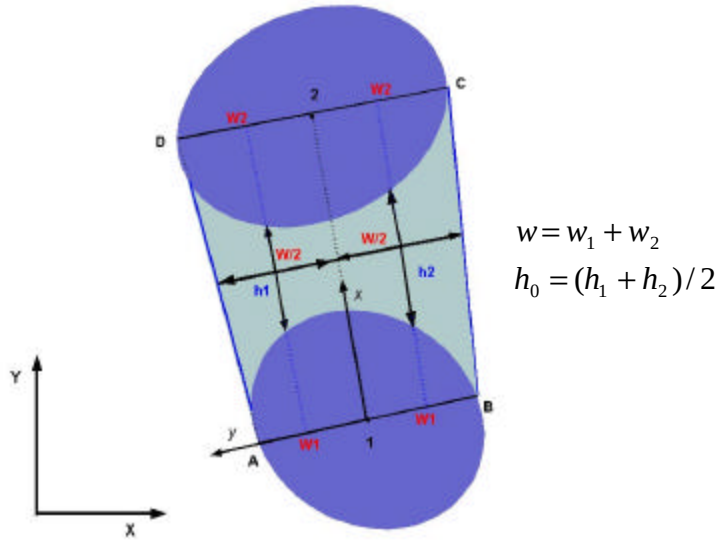

Figure 17. Maximally filled cement binder model.

In order to simulate the fracture and failure behaviors observed in the actual IDT test shown in Figure 14, a fracture criterion was introduced into the damage-softening model. The criteria are based on the binder element stiffness reducing to a sufficiently small value that can be interpreted as failure thus resulting in debonding with the aggregates. The binder fracture criteria for normal/tangential behavior are based on the average fracture strength given by $\sigma_f = c_f \sigma_c$, where c_f is a fracture factor and σ_c is the critical binder strength defined previously. Thus if a binder element softening behavior reduces to a stress level less than σ_f, it will be taken as a failed element and removed from the model system. This scheme has been incorporated into the modeling scheme and applied to the model previously shown in Figure 16 using a fracture factor of $c_f = 0.05$. Figure 18 illustrates the simulation results using this modeling technique for five load steps. Figure 18(a) shows the initial load step and also indicates the initial tension and compression behavior within the micro-frame element network. Figures 18(b)-(e) illustrate the fracture evolution in later load steps. Figure 18(f) shows a fracture pattern observed in the actual laboratory test near the end of loading process. This can be compared with the model prediction

in Figure 18(e). It appears that micromechanical model simulation is in general agreement with test photographic data.

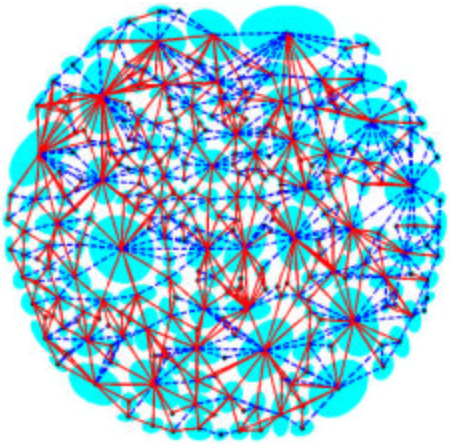

Solid line – Compression element
Dashed line – Tension element

$(a)\ \Delta = 0.5mm$

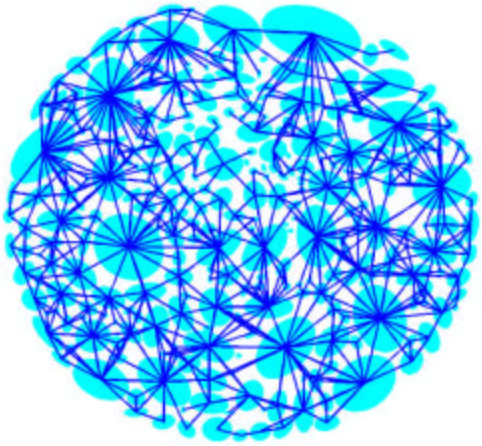

$(b)\ \Delta = 1mm$

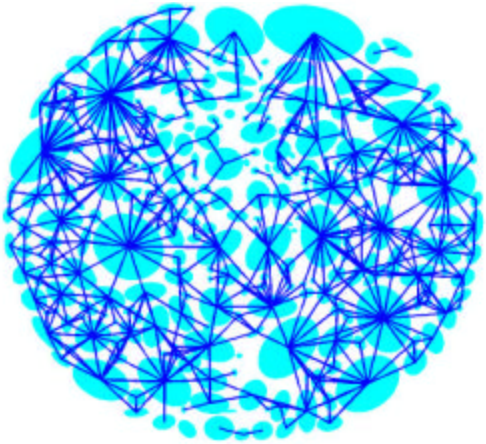

$(c)\ \Delta = 2mm$

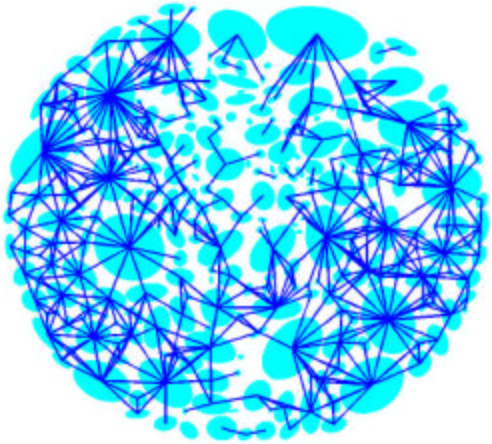

$(d)\ \Delta = 4mm$

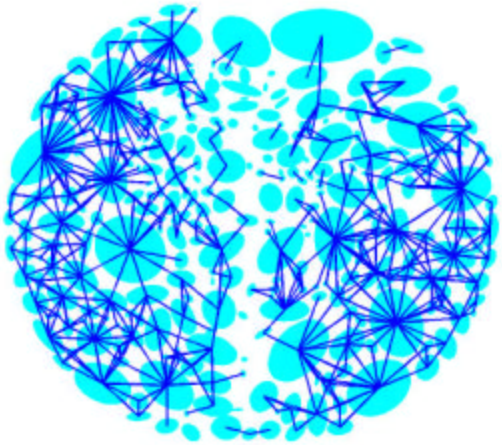

$(e)\ \Delta = 6mm$

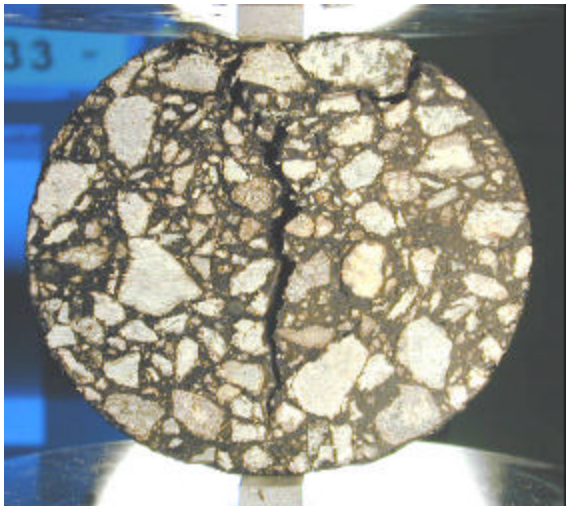

(f) Damaged Specimen

Figure 18. Damaging processes in the IDT simulation.

4. BINDER CHARACTERIZATION TESTING

To predict asphalt behavior, the numerical model requires the characteristics of the binder. In this study the binder is taken to be the material between the aggregates, and this would include the mastic, additives (if any) and the fine material having sub millimeter particle size. Special binder samples having overall size of 44 mm diameter and 50 mm height were prepared with fine material in two different size ranges, 0.075-0.6 mm (sieve size of 200-30) and 0.075-0.3 mm (sieve size of 200-50). The compressive modulus, compressive strength and the splitting strength of these samples were then evaluated.

Identical to the mix parameters used for the asphalt concrete, the samples used for binder characterization also contained 30% recycled asphalt fines. The RAP was sieved and the fine RAP in the appropriate size range was obtained. The total RAP content was 30% with a total asphalt percentage of 5.4%. The virgin asphalt weight was calculated accounting for the binder in the RAP. Following the procedure of Kennedy, et al. (31), a constant compaction force of 6200 lb was applied for 20 minutes at 275^{o} F, after placing the mix in the mold. The samples were then tested at a loading rate of 2.5 mm/minute.

The stress-strain characteristics in compression for both types of samples are shown in Figure 19. These results indicate that the binder Young's modulus was in the range of 72-83 MPa while the compressive strength varied between 2-2.3 MPa. The load-deflection response in the indirect tension test geometry is shown in Figure 20. It was found that the splitting tensile strength of the binder samples were in the range of 0.3-0.38 MPa

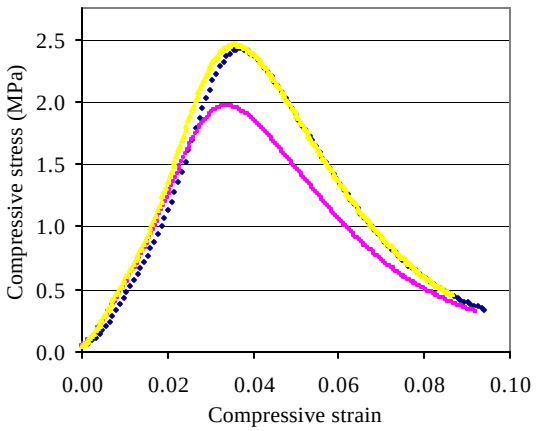

(a) Binder having particles in the 0.075-0.6 mm range. E=83 MPa, Compressive strength= 2.3 MPa

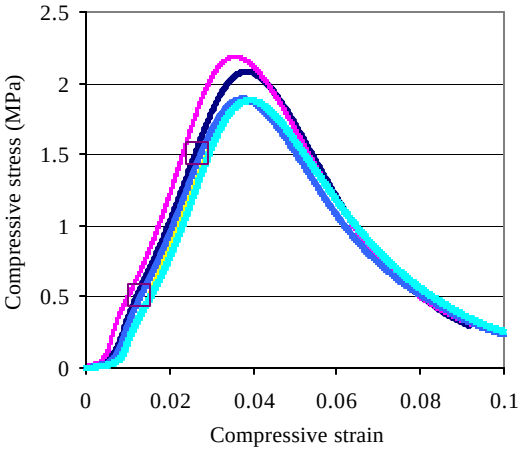

(b) Binder having particles in the 0.075-0.3 mm range, E=72 MPa, Compressive strength =2 MPa

Figure 19. Compressive stress-strain response of binder.

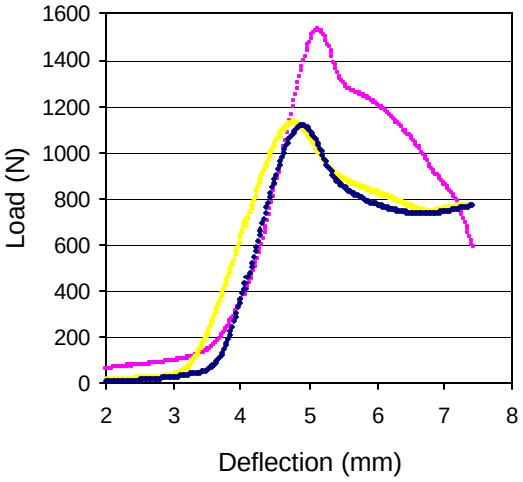

(a) Binder with particles in the range of 0.075-0.6 mm, Average splitting strength = 0.38 MPa

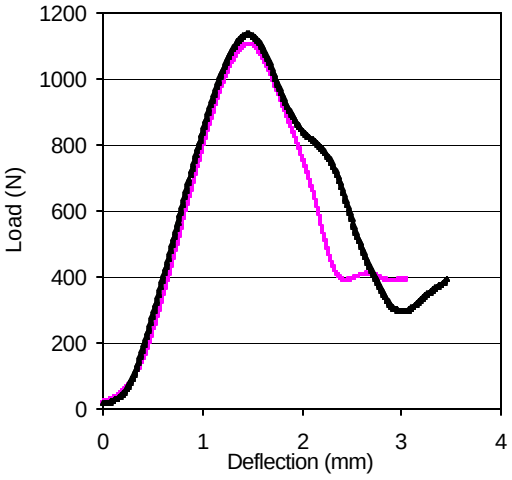

(b) Binder with particles in the range of 0.075-0.3 mm, Average splitting strength = 0.3 MPa

Figure 20. Load deflection characteristics of binder in indirect tension.

5. SUMMARY AND CONCLUSIONS

A two-dimensional micromechanical model has been developed to simulate the behavior of asphalt concrete. The material microstructure composed of aggregates, binder cement and air voids was simulated with an equivalent finite element network that represents the load-carrying behavior between aggregates in the multiphase material. These network elements were specially developed from an elasticity solution for cemented particulates. Incorporating a damage mechanics approach with this solution allowed the development of a softening model capable of predicting typical global inelastic behavior found in asphalt materials. This theory was then implemented within the *ABAQUS* FEA code using the User Defined Element subroutine. In order to create material models, a numerical material generating code was developed that constructs aggregate-binder systems with varying degrees of microstructure.

A series of three models of indirect tension samples were numerically generated. Each model sample was numerically subjected to the loading and constraints of typical IDT tests. Simulation results were then compared with collected experimental data. The overall sample load-deformation simulations compared favorably with the data. The damage model was able to correctly predict the extensive softening behavior found in actual asphalt materials. Finally a brief investigation was made into the evolution of the internal micro-damage within the IDT models. During incremental loading of the sample, all elements within the model were monitored for softening and the evolution of this behavior was recorded. Photographic data from an actual IDT test was collected on the behavior of the surface aggregates and binder damage patterns. Comparisons of the model damage evolution with the experimental photographic data showed reasonable qualitative comparison.

Additional work was reported on developing models from actual asphalt samples. A preliminary investigation was shown whereby a model sample was generated from image analysis of a surface scan of an actual IDT specimen. This model was then numerically

subjected to the IDT loading and comparisons were made with the actual test data. The simulations gave good agreement with the data and qualitatively showed similar fracture/failure patterns within the sample. The current two-dimensional model is limited to assume uniform behavior through the thickness of the simulated sample. Future plans include the development of a three-dimensional model that can more accurately account for the variation in material properties through the thickness of typical laboratory samples.

6. ACKNOWLEDGEMENT

The authors would like to acknowledge supported from the Transportation Center at the University of Rhode Island under Grant FY 01-14. Additional support was also provided from the Northeast Asphalt Institute and Cardi Construction Corporation.

7. PRESENTATIONS AND PUBLICATIONS

Presentations and publications of the work during this project period include:

"Microstructural Simulation of Asphalt Materials: Modeling and Experimental Verification", with Q. Dai, V. Parameswaran, A. Shukla, 15th ASCE Engineering Mechanics Conf., Columbia University, New York, NY, June 2002.

"Microstructural Simulation of Asphalt Materials: Modeling and Experimental Studies", with Q. Dai, V. Parameswaran, A. Shukla, to appear in ASCE Journal of Materials in Civil Engineering.

8. REFERENCES

(1) Dvorkin, J., A. Nur, and H. Yin. Effective Properties of Cemented Granular Materials, Mech.of Materials, Vol.18, 1994, pp. 351-366.
(2) Zhu, H., C.S. Chang and J.W. Rish. Normal and Tangential Compliance for Conforming Binder Contact I: Elastic Binder, Intl. J. Solids Structures, Vol. 33, 1996, pp.4337-4349.
(3) Chang, C.S. and J. Gao. Rheological Modeling of Randomly Packed Granules With Viso-Elastic Binders of Maxwell Type, Comp. and Geotech., Vo. 21, 1997, pp. 41-63.
(4) Cheung, C.Y., A.C.F. Cocks and D. Cebon. Isolated Contact Model of an Idealized Asphalt Mix, Intl. J. Mech. Sci., Vol. 41, 1999, pp.767-792.
(5) Zhu, H. and J.E. Nodes. Contact Based Analysis of Asphalt Pavement with the Effect of Aggregate Angularity, Mech. Of Materials, Vol. 32, 2000, pp. 193-202.
(6) Krishnan, J.M. and C.L. Rao. Mechanics of Air Voids Reduction of Asphalt Concrete Using Mixture Theory, Int. Jour. Eng. Sci., Vol. 38, 2000, pp.1331-1354.
(7) Rothenburg, L., A. Bogobowicz and R. Haas. Micromechanical Modeling of Asphalt Concrete in Connection with Pavement Rutting Problems, Proc. 7th Intl. Conf. On Asphalt Pavements, Vol. 1, 1992, pp. 230-245.

(8) Chang, G.K. and N.J. Meegoda. Simulation of the Behavior of Asphalt Concrete Using Discrete Element Method, Proc. 2nd Intl. Conf. On Discrete Element Methods, M.I.T, 1993, pp. 437-448.
(9) Trent, B.C. and L.G. Margolin. Modeling Fracture in Cemented Granular Materials, ASCE Pub. Fracture Mechanics Applied to Geotechnical Engineering, Proc. ASCE National Convention, Atlanta. 1994.
(10) Buttlar, W.G. and Z. You Discrete Element Modeling of Asphalt Concrete: Micro-Fabric Approach, *Transportation Research Record 1757*, TRB, National Research Council, Washington, D.C., 2001, pp.111-118.
(11) Ullidtz, P. A Study of Failure in Cohesive Particulate Media Using the Discrete Element Method, Proc. 80th Transportation Research Board Meeting, Washington, D.C., 2001.
(12) Sadd, M.H. and J.Y. Gao. The Effect of Particle Damage on Wave Propagation in Granular Materials, *Mechanics of Deformation and Flow of Particulate Materials*, Ed. C.S. Chang, A. Misra, R.Y. Liang and M. Babic, Proc. McNu Conference, Trans. ASCE, Northwestern Univ., 1997, pp.159-173.
(13) Sadd, M.H., and J.Y. Gao Contact Micromechanics Modeling of the Acoustic Behavior of Cemented Particulate Marine Sediments, Proc. 12th ASCE Engineering Mechanics Conf., La Jolla, CA., 1998.
(14) Stankowski, T. Numerical Simulation of Progressive Failure in Particle Composites", Ph.D. Thesis, Univserity of Colorado, 1990.
(15) Sepehr, K., O.J. Harvey, Z.Q. Yue and H.M. El Husswin. Finite Element Modeling of Asphalt Concrete Microstructure, Proc. 3rd Intl. Conf. Computer-Aided Assessment and Control Localized Damage, Udine, Italy., 1994.
(16) Bazant, Z.P., M.R. Tabbara, Y. Kazemi, and G. Pijaudier-Cabot. Random Particle Simulation of Damage and Fracture in Particulate or Fiber-Reinforced Composites, Damage Mechanics in Engineering Materials, AMD Vol 109, Trans. ASME., 1990.
(17) Mora, P. A Lattice Solid Model for Rock Rheology and Tectonics, The Seismic Simulation Project Tech. Rep., Vol. 4, 1992, pp.3-28, Institut de Physique du Globe, Paris.
(18) Sadd, M.H., L. Qiu, W. Boardman, and A. Shukla. Modeling Wave Propagation in Granular Materials Using Elastic Networks", Intl. J. Rock Mech. & Minning Sci, Vol. 29, 1992, pp. 161-170.
(19) Budhu, M., S. Ramakrishnan and G. Frantziskonis Modeling of Granular Materials: A Numerical Model Using Lattices, *Mechanics of Deformation and Flow of Particulate Materials*, Ed. C.S. Chang, A. Misra, R.Y. Liang and M. Babic, Proc. McNu Conference, Trans. ASCE, Northwestern Univ., 1997.
(20) Guddati, M.N., Z. Feng and Y.R. Kim. Towards a Micromechanics-Based Procedure to Characterize Fatigue Performance of Asphalt Concrete, Proc. 81st Transportation Research Board Annual Meeting, Washington, D.C., 2002.
(21) Birgisson, B., C. Soranakom, J.A.L. Napier and R. Roque. Simulation of the Cracking Behavior of Asphalt Mixtures Using Random Assemblies of Displacement Discontinuity Boundary Elements. Proc. 15th ASCE Eng. Mechanics Conf., Columbia Universtiy, 2002.
(22) Bahia, H., H. Zhai, K. Bonnetti and S. Kose. Nonlinear Viscoelastic and Fatigue Properties of Asphalt Binders, J. Assoc. Asphalt Paving Tech., Vol. 68, 1999, pp. 1-34.
(23) Papagiannakis, A.T., A. Abbas and E. Masad. Micromechanical Analysis of the Viscoelastic Properties of Asphalt Concretes, Proc. 81st Transportation Research Board Annual Meeting, Washington, D.C., 2002.
(24) Mustoe, G.G.W. and D.V. Griffiths. An Equivalent Model Using Discrete Element Method (DEM), Proc. 12th ASCE Engineering Mechanics Conf., La Jolla, CA., 1998.
(25) Sadd, M.H. and Q.L. Dai. Effect of Microstructure on the Static and Dynamic Behavior of Recycled Asphalt Material, Year 1 Final Report #536108, University of Rhode Island Transportation Center, 2001.
(26) Ishikawa, M., H. Yoshikawa and T. Tanabe The Constitutive Model in Terms of Damage Tensor, Proc. Of Finite Element Analysis of Reinforced Concrete Structures, ASCE Publication, Tokyo, 1986, pp.93-103.
(27) Zhong, X. and C.S. Chang. Micromechanical Modeling for Behavior of Cementitious Granular Materials, J. Eng. Mechanics, ASCE, Vol. 125, 1999, pp.1280-1285.

(28) Sadd, M.H., Shukla, A., Parameswaran, V. and Q. Dai, Effect of Microstructure on the Static and Dynamic Behavior of Recycled Asphalt Material, University of Rhode Island Transportation Center Report # 536138, July 2002.
(29) DIPimage - A Scientific Image Toolbox for MATLAB, http://www.ph.tn.tudelft.nl/DIPlib
(30) Fitzgibbon, A., M. Pilu and R. Fisher. Direct Least-Square Fitting of Ellipse, International Conference on Pattern Recognition, Vienna, 1996.
(31) Kennedy, T.W., Roberts, F.L. and K.W. Lee, Evaluation of Moisture Susceptibility of Asphalt Mixtures using Texas Freeze-Thaw Pedestal Test, Proc. of the Association of Asphalt Paving Technologists, Vol. 51, pp. 327-341, Kansas City, MO, 1982.